A python library for computing individual and merged non-CO_2 algorithmic climate change functions: CLIMaCCF V1.0

Simone Dietmüller[1], Sigrun Matthes[1], Katrin Dahlmann[1], Hiroshi Yamashita[1], Abolfazl Simorgh[2], Manuel Soler[2], Florian Linke[3,4], Benjamin Lührs[3], Maximilian M. Meuser[3,4], Christian Weder[3], Volker Grewe[5,1], Feijia Yin[5], and Federica Castino[5]

[1]Deutsches Zentrum für Luft und Raumfahrt, Institut für Physik der Atmosphäre, Oberpfaffenhofen, Germany
[2]Department of Aerospace Engineering, Universidad Carlos III de Madrid, Spain
[3]Hamburg University of Technology (TUHH), Hamburg, Germany
[4]Deutsches Zentrum für Luft und Raumfahrt, Air Space Transportation Systems, Hamburg, Germany
[5]Faculty of Aerospace Engineering, Delft University of Technology, Delft, the Netherlands

Correspondence: S. Dietmüller (simone.dietmueller@dlr.de)

Abstract. Aviation aims to reduce its climate impact by adopting trajectories, that avoid those regions of the atmosphere where aviation emissions have a large impact. To that end, prototype algorithmic climate change functions (aCCFs) can be used, which provide spatially and temporally resolved information on aviation's climate impact in terms of future near-surface temperature change. These aCCFs can be calculated with meteorological input data obtained from e.g. numerical weather prediction models. We here present the open-source Python Library called CLIMaCCF, an easy to use and flexible tool which efficiently calculates both the individual aCCFs (i.e., water vapour, nitrogen oxide (NO_x) induced ozone and methane, and contrail-cirrus aCCFs) and the merged non-CO_2 aCCFs that combine all these individual contributions. These merged aCCFs can be only constructed with the technical specification of aircraft/engine parameters, i.e., NO_x emission indices and flown distance per kg burnt fuel. These aircraft/engine specific values are provided within CLIMaCCF version V1.0 for a set of aggregated aircraft/engine classes (i.e. regional, single-aisle, wide-body). Moreover, CLIMaCCF allows by a user-friendly configuration setting to choose between a set of different physical climate metrics (i.e. average temperature response for pulse or future scenario emissions over the time horizons of 20, 50 or 100 years). Finally, we demonstrate the abilities of CLIMaCCF by a series of example applications.

1 Introduction

Global aviation significantly contributes to the anthropogenic climate change by CO_2 and non-CO_2 emissions. Non-CO_2 emissions also affect the climate system by changing the concentrations of ozone, water vapour, methane and aerosols as well as cloudiness by forming contrail-cirrus. As recently reviewed by Lee et al. (2021), global aviation contributes to 3.5% of the total anthropogenic radiative forcing (RF). The total aviation RF comprises about one third CO_2 effects and about two thirds non-CO_2 effects. The largest single contribution to aviation RF comes from contrails and contrail-cirrus, but this estimate is affected by a very large uncertainty, as well as for NO_x impacts (Grewe et al., 2019). In contrast to the CO_2 impact, the non-CO_2 impacts reveal a strong dependence on atmospheric conditions. Thus, the non-CO_2 impacts depend on the geographical

location, altitude and time of aircraft emission (e.g. Grewe et al., 2014; Frömming et al., 2021). In order to provide information on this spatially and temporally resolved climate impact of these non-CO_2 effects, climate change functions (CCFs) were developed with an atmospheric chemistry climate model system (Frömming et al., 2021). These CCFs provide a measure of the

25　spatial and temporal climate impact for a given emission by using the metric of average temperature response (ATR). These CCFs were calculated for a wide range of time steps and for eight representative weather types in summer and winter classified after Irvine et al. (2013) over the North Atlantic region (Frömming et al., 2021).

Based on these CCFs, Grewe et al. (2014) investigated the transatlantic air traffic for one single winter day and analysed the routing changes that are required to achieve a reduction in the impact of air traffic on climate. Thus, this study provides a

30　first comprehensive and valuable basis for weather-dependent flight trajectory optimization with minimum climate impact. However, as the calculation of these CCFs within a global chemistry climate model system requires large computational cost, it cannot be used for operational climate optimized flight planning. To address this issue, the initial concept of CCFs was extended to algorithmic climate change functions (aCCFs). These functions provide a very fast computation of the individual non-CO_2 climate impact as they are based on mathematical formulas which only need a fairly limited number of relevant local

35　meteorological parameters as input (e.g Matthes et al., 2017; van Manen and Grewe, 2019; Yin et al., 2022). To derive the mathematical formulation of the individual aCCFs (a detailed formulation of these prototype aCCFs is given in Appendix A), statistical methods were used. A detailed explanation of the concept of aCCFs approach can be found in van Manen and Grewe (2019) for the NO_x induced species ozone and methane, and for water vapour. In the case of the contrail aCCFs approach, a detailed description is available in the supplement of Yin et al. (2022). These aCCFs formulas facilitate predicting the climate

40　impact of individual species by means of meteorological input data from e.g., weather forecast, without computationally extensive re-calculation using chemistry-climate models. Of course, a number of assumptions and simplifications are necessary for this kind of approach. Nevertheless, it was shown in the studies of van Manen and Grewe (2019) and Yin et al. (2022) that these prototype aCCFs are in broad agreement with the climate change metric of earlier studies, i.e. CCFs (Frömming et al., 2021).

45　Indeed, aCCFs can be used for trajectory planning purposes. The weather dependent re-routing of flight trajectories in order to reduce the climate impact of air traffic needs the information on regions that are highly sensitive to aviation emissions. In order to quantify the potential of mitigating aviation's climate impact, case studies with optimized aircraft trajectories that use the above described aCCFs, were performed. These studies showed that re-routing has a large potential to reduce the air traffic's contribution to climate change. Even small changes in the flight trajectory can lead to significant reduction of the climate

50　impact (see e.g. Matthes et al., 2017, 2020; Lührs et al., 2021; Castino et al., 2021; Rao et al., 2022).

Nevertheless, a climate optimal trajectory (interested readers are also referred to Simorgh et al. (2022) for a recent, thorough survey on climate optimal aircraft trajectory planning) requires a quantitative estimate of the total non-CO_2 climate impact as four dimensional data set (latitude, longitude, altitude, time). This location and time dependent quantitative estimate can be generated by combining the individual aCCFs of water vapour, NO_x induced ozone and methane changes, and contrail-cirrus

55　to a merged non-CO_2 aCCF by means of a consistent climate metric. However, for combining the individual aCCFs, it has to be considered that the aCCF algorithms provide their estimates in average temperature change per emitted mass of the relevant

species, e.g. in K/kg(NO_2) for the ozone aCCF. Thus, before merging the individual aCCFs, all individual aCCFs have to be converted to the unit of K/kg(fuel). For this conversion the information on NO_x emission indices and flown distance per kg burnt fuel (specific range) is needed. Based on these generated merged non-CO_2 aCCFs climate optimized trajectories that

60   aim to avoid climate sensitive regions can be calculated efficiently. Note, that also the total merged aCCF (non-CO_2 as well as CO_2 effects included) can be calculated, however as the CO_2 aCCF is a constant in location and time, we focus on the merged non-CO_2 aCCFs.

The development of the Python Library, CLIMaCCF, which will be released together with this paper (available on Zenodo with the software DOI: 10.5281/zenodo.6977272) represents a technical enabler to seamlessly integrate the information of spatially

65   and temporally dependent non-CO_2 climate impacts (in terms of individual and also merged non-CO_2 aCCFs) in a trajectory optimization tool. In this paper we will present both the scientific background of merging aCCFs and the technical framework of the user friendly and flexible Python Library CLIMaCCF V1.0.

The paper is structured as follows. In Section 2 the scientific background of generating merged aCCFs, which quantify the

70   spatial and temporal non-CO_2 climate impact of aviation, is described. Merged non-CO_2 aCCFs rely on the individual prototype algorithmic climate change functions. Before combining these individual aCCFs to a merged aCCF, assumptions about emission indices of NO_x and flown distance per kg burnt fuel have to be made and decisions on the physical climate metric used and the inclusion or exclusion of the forcing dependent efficacy (e.g. Hansen et al., 2005) have to be taken. In Section 3 the technical implementation (general architecture) of the Python Library CLIMaCCF is given by describing how the user can

75   generate individual and merged aCCFs in a flexible manner. Section 4 provides various analyses of the individual aCCFs and the merged aCCF, showing their characteristic patterns. Moreover the sensitivity of merged aCCFs to different assumptions, as well as the identification of climate highly sensitive regions is given. A discussion about the capability and the limitations of the Python Library follows (Section 5), before the conclusions are drawn in Section 6.

2   Generation of merged aCCFs

80   Based on aCCFs that represent the individual effects of water vapour, NO_x induced ozone and methane changes and contrail-cirrus, a single aCCF function which combines these individual CO_2 and non-CO_2 impacts can be generated (i.e. merged aCCF). This merged aCCF can be used as advanced meteorological (MET) information for flight planning, as a climate-optimized trajectory requires the quantification of the total climate impact as four-dimensional data set (latitude, longitude, altitude and time). Such a merged aCCF can only be constructed by using assumptions on several aircraft/engine specific

85   parameters and consistent climate metrics. In the following we describe the concept of merging aCCFs and the underlying assumptions in detail.

2.1 Mathematical formulation of individual aCCFs

As mentioned in the introduction, aCCFs were developed to provide a computational fast way to calculate the climate impact of individual non-CO_2 aviation emissions in dependence of their geographical location, altitude, time and weather. Correlations and statistical methods were used to derive the individual prototype aCCFs of water vapour, NO_x induced ozone, NO_x induced methane and contrail-cirrus. For water vapour, ozone and methane aCCFs, this was done by linking a large range of climate change function data, which were calculated in a detailed chemistry climate model simulation (Frömming et al., 2021), to selected meteorological data, as e.g., temperature or geopotential height (van Manen and Grewe, 2019). The algorithm for contrail aCCFs was developed differently. Contrail aCCFs are obtained from contrail radiative forcing calculations which are based on ERA-Interim reanalysis data (Dee et al., 2011) and on contrail trajectory data (Yin et al., 2022). A short overview of the mathematical formulation of these emission type dependent prototype aCCFs is given in Appendix A of this document. For a detailed description of the first complete and consistent set of prototype aCCFs (aCCF-V1.0) the reader is referred to Yin et al. (2022). Moreover, within the EU project FlyATM4E an updated set of aCCFs (aCCF-V1.1) was developed that considers current level of scientific understanding of aviation's climate effects: For more details, readers are referred to Matthes et al. (2022, in preparation).. Overall for the development of the aCCF a number of assumptions and simplifications were necessary. Nevertheless, it was shown that these aCCFs are in broad agreement with the climate change metric of earlier studies (e.g. van Manen and Grewe, 2019; Yin et al., 2022).

2.2 Merged non-CO_2 aCCFs and total aCCFs

To build the merged non-CO_2 aCCFs, all individual aCCFs are converted consistently to the same physical units of [K/kg(fuel)]. Note that the individual aCCFs (except the water vapour aCCF) are given in different units, i.e., K/km for contrail aCCFs or K/kg(NO_2) for the NO_x induced ozone and methane aCCF. These differences result in different weighting of the effect for different aircraft/engine classifications. To this end, we select for NO_x emission indices (EI_{NO_x} in g(NO_2)/kg(fuel)) and for contrail cirrus specific range or flown distance per kg burnt fuel (F_{km} in [km/kg(fuel)]). Note that the water vapour aCCF formula is already fuel related and, thus, does not need to be multiplied by the emission index of water vapour. Typical transatlantic fleet mean values of EI_{NO_x} and of F_{km} are available from the literature: transatlantic fleet mean values for F_{km} is 0.16 km/kg(fuel) (Graver and Rutherford (2018) and personal communication F. Linke, TU Hamburg, 2020) and for EI_{NO_x} is 13 g (NO_2)/kg(fuel) (e.g. Penner et al., 1999), respectively. Another possibility is to take specific emitted amounts of NO_x emissions and fuel consumption values from an engine performance model. Here, we use altitude depending mean emission indices for NO_x and flown distance per kg burnt fuel for aggregated aircraft/engine classifications (e.g. regional, single-aisle and wide-body, see Section 2.3) and combine that with the choice of climate metric (Section 2.4) and the use of efficacies

(Section 2.5) to merge non-CO_2 aCCFs:

$$aCCF_{merged}^{non-CO_2}(t,x,y,z,i_{ac},i_r,i_{CM}) = \tag{1}$$

$$aCCF_{O_3}(t,x,y,z) * EI_{NO_x}(i_{ac},z) * r_{O_3}(i_r) * CM_{O_3}(i_{CM})$$

$$+aCCF_{CH_4}(t,x,y,z) * EI_{NO_x}(i_{ac},z) * r_{CH_4}(i_r) * CM_{CH_4}(i_{CM})$$

$$+aCCF_{PMO}(t,x,y,z) * EI_{NO_x}(i_{ac},z) * r_{PMO}(i_r) * CM_{PMO}(i_{CM})$$

$$+aCCF_{contrail}(t,x,y,z) * F_{km}(i_{ac},z) * r_{contrail}(i_r) * CM_{contrail}(i_{CM})$$

$$+aCCF_{H_2O}(t,x,y,z) * r_{H_2O}(i_r) * CM_{H_2O}(i_{CM}),$$

where $aCCF_X$ are the algorithmic climate change functions for a specie X i.e., water vapour (H_2O), ozone (O_3), methane (CH_4), primary mode ozone (PMO), and contrail-cirrus. The variables t,x,y,z indicate the three spatial variables (x,y,z) and time (t). i_{ac} is the identifier for three mean aircraft/engine classes: regional, single-aisle, wide-body (see Section 2.3). $r_X(i_r)$ is the efficacy (see Section 2.5) of the species X with the switch $i_r \in \{0,1\}$ for disregarding or using the efficacies (i.e. $r_X(0)$=1) and $CM_X(i_{CM})$ is the climate metric conversion factor (see Section 2.4) for species X and the choice of currently four climate metrics $i_{CM} \in \{0,1,2,3\}$.

By additionally including the aviation climate impact of CO_2 the total merged aCCF is given:

$$aCCF_{merged}^{total}(t,x,y,z,i_{ac},i_r,i_{CM}) = \tag{2}$$

$$= aCCF_{CO_2} * CM_{CO_2}(i_{CM}) + aCCF_{merged}^{non-CO_2}(t,x,y,z,i_{ac},i_r,i_{CM})$$

Note that the CO_2 aCCF is independent of the location x,y,z, efficacy (r_X) and aircraft class.

For a merged aCCF it is required that the individual aCCFs are based on the same physical climate metric, emission scenario and time horizon. The recent publication of Yin et al. (2022) comprises such a consistent set of individual updated prototype aCCFs. Note, that earlier publications (as e.g. Yamashita et al. (2020)) provided mathematical formulations that assumed different emission scenarios for water vapour and NO_x aCCFs and for contrail aCCFs , as they were developed separately.

Overall, merged aCCFs are not only a function of time and location, but also a function of aircraft/engine specific data, climate metric and efficacy. For an efficient and flexible provision of such merged aCCFs we developed the Python Library CLIMaCCF.

2.3 Choice of aircraft/engine specific parameters

The calculation of merged non-CO_2 aCCFs requires knowledge about the emission index of NO_x, EI_{NO_x}, and the flown distance per kg burnt fuel, F_{km} (see Eq. 1). As these indices vary depending on the actual aircraft-engine combination (i_{ac}) and the cruise altitude (z), the use of global mean emission indices should be avoided. Moreover, there is a strong altitude dependency of the NO_x emission index and flown distance F_{km}, which should be considered as well. Aggregated values for emission indices are derived from trajectory simulation and emission inventory data. Similarly, aggregated values for the specific range (i.e. flown distance per kg burnt fuel) F_{km}, are gained.

For instance, analyzing the ten most frequented routes in the North Atlantic Flight Corridor with the ten most used aircraft types in 2012 yields an average flown distance per kg burnt fuel of 0.16 km/kg(fuel) (personal communication F. Linke, 2020) for transatlantic flights. More differentiated values are obtained by analyzing available emission inventory data from the DLR project "Transport and Climate" (TraK). This data contains the air traffic emission distribution in year 2015 and can be evaluated separately per aircraft type, altitude or region. Basis for the development of these emission inventories was a database of reduced emission profiles within the Global Air Traffic Emission Distribution Laboratory (GRIDLAB, Linke et al. (2017)). Those profiles were created by simulating aircraft trajectories for various ranges and load conditions with aircraft performance models from EUROCONTROL's Base of Aircraft Data (BADA, Nuic and Mouillet (2012)) model families 3 and 4. Along those trajectories engine emissions were calculated using the EUROCONTROL-modified Boeing Fuel Flow method 2 (DuBois and Paynter, 2006; Jelinek, 2004) applied to engine certification data for the Landing and Take-off Cycle (LTO) taken from the International Civil Aviation Organization (ICAO) Engine emission database. In order to create the reduced profiles, those trajectory emission data were finally resampled to only consider key points along the profile such as transitions between flight phases. The emission inventory contains gridded data in a resolution of $0.25° \times 0.25° \times 1000$ ft (Weder et al., 2022, under preparation). Associated to each grid cell are the amounts of the individual emission species as well as the flown distance in that grid cell. The aggregated mean EI_{NO_x} value at a given altitude is calculated by dividing the sum of the amounts of emissions per species in all grid cells at that altitude by the sum of burnt fuel at that altitude. The specific range is calculated accordingly. We evaluated aggregated fleet-level values for $EI_{NO_x}(i_{ac}, z)$ and the specific range $F_{km}(i_{ac}, z)$ for a variety of aircraft/engine classes. As the aircraft specific values are similar for certain aircraft/engine class, we group those aircraft classes and provide their average fleet values in Tables 1 and 2. Three different aircraft types are given: regional (small aircraft with short range (up to 100 seats)), single-aisle (short to medium-range narrow-body aircraft), wide-body (medium to long-range aircraft (250-600 seats)) .

Table 1. Average specific NO$_x$ emission indices (in g(NO$_2$)) for the three aircraft classes (regional, single-aisle, wide-body) derived from the global TraK emission inventory. $EI_{NO_x}((i_{ac}, z))$ are shown for various typical flight altitudes (20000 ft - 40000 ft). Besides the flight altitude in ft the corresponding pressure level under ICAO standard atmosphere is given in hPa.

flight altitude [ft]	pressure level [hPa]	regional [g(NO$_2$)]	single-aisle [g(NO$_2$)]	wide-body [g(NO$_2$)]
20000	466	11.628	17.279	24.750
25000	376	10.223	14.877	22.182
30000	301	9.377	13.603	19.158
35000	238	7.968	11.249	15.008
40000	188	6.567	8.564	12.730

Table 1 clearly shows that average EI_{NO_x} values increase with increasing aircraft class/size, while EI_{NO_x} values decrease with increasing altitude. NO$_x$ emissions are produced during combustion due to high combustion temperatures, which are

Table 2. Average flown distance per burnt fuel (km/kg(fuel)) for the three aircraft classes (regional, single-aisle, wide-body) derived from the global TraK emission inventory. $F_{km}(i_{ac}, z)$ values are shown in dependence of typical flight altitude (20000 ft - 40000 ft). Besides the flight altitude in ft the corresponding pressure level under ICAO standard atmosphere is given in hPa.

flight altitude [ft]	pressure level [hPa]	regional [km/kg(fuel)]	single-aisle [km/kg(fuel)]	wide-body [km/kg(fuel)]
20000	466	0.393	0.252	0.096
25000	376	0.442	0.282	0.107
30000	301	0.470	0.287	0.117
35000	238	0.488	0.324	0.120
40000	188	0.682	0.401	0.157

connected to high thrust settings and engine load conditions. In general, the thrust requirement increases with the aircraft size. Increasing the thrust requirement leads to an increase in the combustion temperature, therefore, an increase in NO_x emissions. Below cruise altitude the aircraft is e.g. during climb operated with climb thrust and during descent with near idle conditions leading to on average higher engine loads at lower altitudes than during cruise. The flown distance in Table 2 increases with
175 altitude, as the aircraft is operated in near-fuel-optimal conditions during cruise. On the other hand, larger aircraft tend to have a lower specific range than aircraft with shorter range, as they become less fuel efficient on longer ranges, on which they have to carry additional fuel solely for the purpose of transporting a higher fuel mass over a long distance.

2.4 Choice of physical climate metric

Physical climate metrics can be understood as methods to directly compare the climate impact of different forcing agents,
180 or different sectors and sources (Fuglestvedt et al., 2010). A climate metric is a combination of climate indicator (e.g. average temperature response (ATR) or global warming potential (GWP)), time horizon (e.g. 20, 50 or 100 years) and emission scenario, including emission scenarios and background emission (Fuglestvedt et al., 2010). As emission scenarios a pulse, sustained or a future increasing scenario might be considered (Grewe and Dahlmann, 2015). The choice of an adequate climate impact metric depends on the specific question of climate impact (e.g. 'Contribution to nowadays climate impact', 'What is the
185 long-term climate impact?') to be answered (Grewe and Dahlmann, 2015). Thus, depending on the question different climate impact metrics should be used.

The aCCFs were developed based on the climate metric of average temperature response over a time horizon of 20 years (ATR20). The emission scenario assumed was either based on pulse emission (P) or on the future business as usual emission
190 scenario (F). This inconsistency has been discovered and a revision of the aCCFs is given in the recent publication of Yin et al. (2022). Now all direct outputs of aCCF formulas are given in P-ATR20 (ATR20 based on pulse emission). As P-ATR20 is not well suited for some questions this climate metric is not well suited. Therefore we introduced conversion factors $CM_X(i_{CM})$ (see Eq. 1) which make it possible to switch from the P-ATR20 metric (which is the basis of the aCCF-V1.0 formulas in

the Appendix A) to other physical climate metrics, as e.g. ATR based on the future emission scenario (i.e. business as usual)

195 with different time horizons (i.e. F-ATR20, F-ATR50 or F-ATR100). To calculate these conversion factors we use the non-linear climate response model AirClim (Grewe and Stenke, 2008; Dahlmann et al., 2016) and perform several simulations with different emission scenarios. A first set of conversion factors for four different metrics (i_{CM}) is presented in Table 3. Conversion factors for other emission scenarios and other climate indicators will be presented in an upcoming publication by Dahlmann et al., 2022 (in preperation).

Table 3. Climate metric conversion factors CM_x from P-ATR20 (pulse emission based ATR over 20 years) to F-ATR20 (future emission based ATR over 20 years), F-ATR50 (future emission based ATR over 50 years) and F-ATR100 (future emission based ATR over 100 years) for water vapour, ozone, methane, primary mode ozone (PMO), contrail-cirrus and CO_2 aCCFs.

	F-ATR20	F-ATR50	F-ATR100
water vapour aCCF	14.5	34.1	58.3
ozone aCCF	14.5	34.1	58.3
methane aCCF	10.8	42.5	98.2
PMO aCCF	10.8	42.5	98.2
contrail aCCF	13.6	30.16	48.9
CO_2 aCCF	9.4	44.0	125.0

2.5 Choice of climate forcing related efficacy

200

Radiative forcing (RF), measured in W/m^2, describes the change of the planetary energy balance. RF is often used as metric for comparing the global climate impact of specific forcing components (e.g. CO_2, ozone, aerosols). What makes RF so useful for comparison is its empirical based linear relationship to the steady-state global mean near-surface temperature change. The model dependent constant, which relates these two parameters, is the so-called climate sensitivity parameter λ (e.g. Hansen

205 et al., 2005; Cess et al., 1989). This relation is a good approximation for many spatially homogeneously distributed climate forcing components, such as CO_2. However, for radiatively active gases with a distinctly inhomogeneous structure like, e.g. ozone and contrails, the relation with constant climate sensitivity parameter fails (e.g. Joshi et al., 2003; Hansen et al., 2005). Several studies showed that the RF of some non-CO_2 forcing agents is less or more effective in changing global mean temperature per unit forcing compared to the response of CO_2 forcing. A way to account for this is to introduce a forcing dependent

210 efficacy, which is defined as warming per unit global average forcing divided by the warming per unit forcing from CO_2. By considering this efficacy (Hansen et al., 2005; Ponater et al., 2006; Lee et al., 2021), a better prediction of the global temperature change is given.

As mentioned before, aCCFs are based on the climate metric average temperature response (ATR) over a certain time horizon, a useful metric to asses aviation induced climate impact (Dahlmann et al., 2016). However, here ATR was calculated without

215 taking the efficacy of the different non-CO_2 forcing components into account. Integrating the efficacies r_X of water vapour,

Table 4. Overview of state-of-the-art efficacies r_X of NO_x induced ozone, methane. PMO, as well as of water vapour and contrails. Respective references are given in the right side of the table.

	efficacy	Reference
ozone	1.37	Ponater et al. (2006)
methane	1.18	Ponater et al. (2006)
PMO	1.18	Lee et al. (2021)
H_2O	1	Lee et al. (2021)
contrail-cirrus	0.59	Ponater et al. (2005)
	0.31	Rap et al. (2010)
	0.35	Bickel et al. (2020)
	0.42*	Lee et al. (2021)

* Lee et al. 2021 value is the mean over the values given by Bickel et al. (2020); Ponater et al. (2005); Rap et al. (2010)

ozone, methane and contrail cirrus to the merged aCCFs (see Eq. 1) makes the prediction of aviation climate impact more reliable. State-of-the-art efficacies were recently summarized in Lee et al. (2021) and are shown in Table 4. The efficacy of the NO_x induced short term ozone, NO_x induced methane and NO_x induced primary mode ozone PMO is larger than 1. This means that ozone and methane RF have a higher impact on the temperature response than CO_2. For contrails, the efficacy given

220 in Lee et al. (2021) is lower than 1, meaning that contrail RF has a lower impact on the global temperature response than CO_2. Note that the contrail efficacy of 0.42 in Lee et al. (2021) is based on three different contrail efficacy estimates from earlier studies, including an estimate of 0.59 (Ponater et al., 2005), an estimate of 0.31 (Rap et al., 2010) and an estimate of 0.35 (Bickel et al., 2020).

3 Technical implementation of individual and merged aCCFs in the Python Library CLIMaCCF Version 1.0

225 The generation of individual and merged non-CO_2 aCCFs will be performed by using a user-friendly Library developed with Python, called CLIMaCCF. The scope of CLIMaCCF is to provide individual and merged aCCFs as spatially and temporally resolved information considering meteorology from the actual synoptical situation, the engine/aircraft type, the selected physical climate metric, and the selected version of prototype algorithms in individual aCCFs (i.e. aCCF-V1.0 and aCCF-V1.1; see Section 2.1). In the following, some details on the technical implementation of the Python Library are presented. For a

230 more comprehensive documentation, the reader is referred to the CLIMaCCF User Manual that is provided as a Supplement to this paper. Overall, the Python Library consists of three main blocks: input block, processing block, and output block (see schematic workflow in Figure 1). In the input block, the Python Library obtains the weather data (e.g., forecast, reanalysis, etc.) containing the required meteorological input and configurations like climate metric and aircraft/engine class. In the processing

block, the individual aCCFs are calculated and merged aCCFs are generated. In the output block the individual and merged

235 aCCFs are stored. In the following we describe these three blocks in more detail.
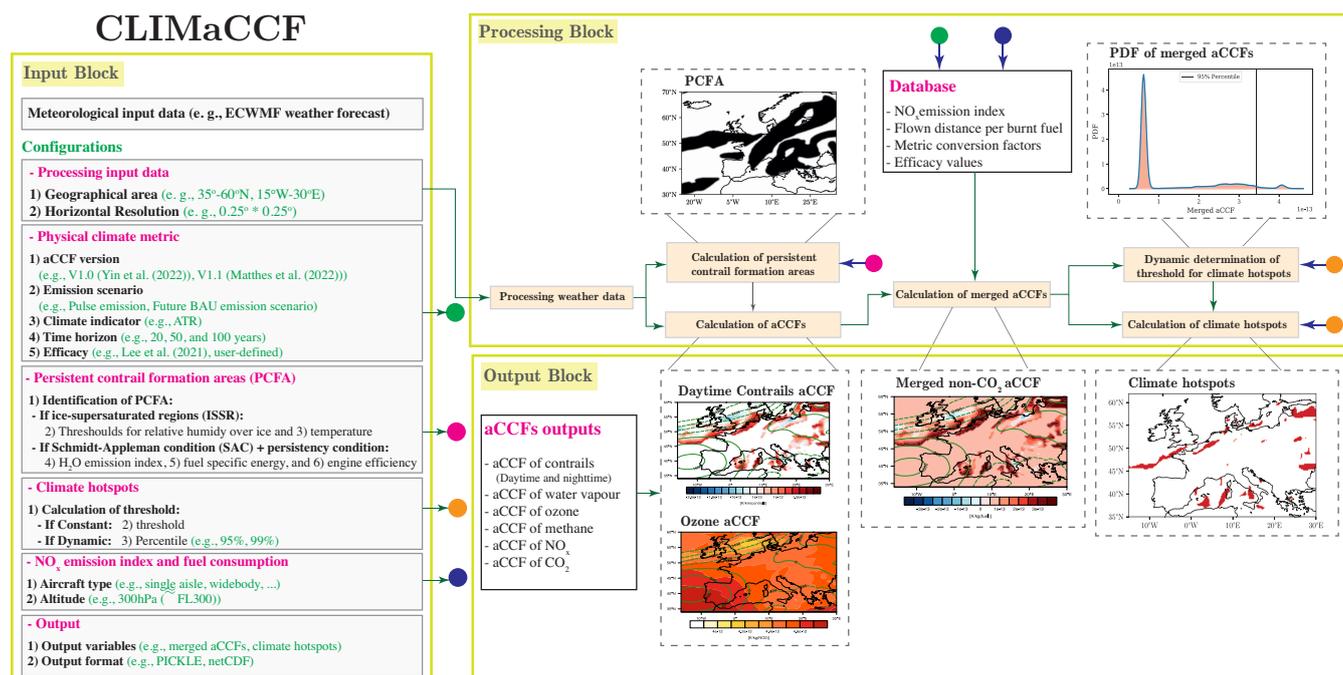
Figure 1. Schematic workflow of calculating individual and merged aCCFs using the Python Library CLIMaCCF Version 1.0. The left box describes the input block, the upper right box the processing block and the lower left box the output block.

3.1 Input block

Within the input block (left box in Fig. 1), the meteorological input data needed to calculate aCCFs are specified by the user. All meteorological input data needed to calculate the individual aCCFs are summarized in Table 5. The current implementation of the Library is compatible and tested with the standard of European Centre for Medium-Range Weather Forecasts (ECMWF)

240 data. These user settings include the selections of geographical area, horizontal resolution and several output options (e.g. the output file can include merged aCCFs, individual aCCFs and the input data used). Besides the specification of meteorological input data, users can select the version of aCCFs they aim to use. These options include aCCF-V1.0, which is the first consistent and complete set of aCCFs (Yin et al., 2022), aCCF-V1.1, in which the aCCFs-V1.0 are scaled by educated guess factors (Matthes et al., 2022, in preparation). Additionally user-defined scaling factors can be applied to the selected aCCF version.

245 These scaling factors are set to one per default, however if a scaling of the aCCFs (to higher or lower values) is wanted (e.g. for sensitivity studies) the user can adopt them accordingly. User settings for the generation of individual and merged aCCFs can also be selected. Here the user can choose different assumptions for aircraft specific parameters and the physical climate metric (emission scenario, physical climate indicator, time horizons). Moreover, the user can decide if the aCCF calculation is

performed with or without considering efficacy. As for efficacy, users can use the values reported by Lee et al. (2021) or define

250 the factors themselves. As the selection of aircraft type/engine is an important factor in determining reliable merged aCCF (see Section 2), we have implemented an initial set of specific emission indices for some selected aircraft/engine combinations. By selecting an aggregated aircraft/engine type, tabulated flight level dependent NO_x emission indices and flown distance per burnt fuel values are used to calculate the merged aCCFs. An additional functionality is the identification of areas that are very sensitive to aviation emission, in the following called 'climate hotspots'. To quantify these areas a threshold value is used to

255 identify the regions with very large effects induced from aviation, has to be chosen. The threshold to determine these climate hotspot areas is also considered as an adjustable parameter (for details, see Section 4). In the end, the users can specify output parameters such as merged aCCFs or the aCCFs of each species. In the case of using ensemble forecasts, one can also receive the ensemble mean and ensemble spread of the resulting individual or merged aCCFs from CLIMaCCF. The user can select the output format (either netCDF, or PICKLE). There is also a possibility to output the climate hotspots in the GeoJSON file

260 format.

3.2 Processing block

The processing block (upper right box in Fig. 1) performs the aCCF calculations using the given weather data and the above-described user settings. The processing block includes, for the aCCF calculation, preprocessing of input variables, the calculation of individual and merged aCCF, as well as the calculation of climate sensitive regions (climate hotspots). A more detailed

265 description of these calculations is given in the following.

Before calculating individual and merged aCCFs, preprocessing of several input data is needed:

Processing weather data: In an initial step, based on the user preferences, the geographical areas, where the merged aCCFs are calculated, can be reduced, or the default resolutions can be changed. In these cases, some modifications are applied to the

270 original input weather data. Notice that the horizontal resolution cannot be increased, and the decrease in resolution is a factor i of natural numbers. For instance, if the resolution of meteorological input data is $0.25° \times 0.25°$, the resolution can be reduced to $i*0.25° \times i*0.25°$, for $i \in \mathbb{N}$.

Calculate required weather variables form alternative variables: If meteorological variables are missing in the input data set, they can be retrieved from provided default data set. However only, if alternative variables described in Table 5 exist in the

275 data set, as they will be employed to calculate required variables.

Tabulated aircraft/engine specific parameters: In the database of the Library, NO_x emission indices (EI_{NO_x}) and flown distances (F_{km}) are provided for different types of aircraft (i.e. regional, single aisle, wide-body) at different flight levels. By using spline interpolations, these indices are calculated for any given flight level (or pressure level).

Calculate persistent contrail formation areas: The units of the day- and night-time contrail aCCFs are given in the unit of

280 [K/km], meaning that they are defined only in areas where the formation of persistent contrails is possible, called persistent contrail formation areas (PCFA). These regions are identified by two atmospheric conditions (e.g. Gierens et al., 2020): First the Schmidt-Appleman condition (SAC) (Appleman, 1953), using the meteorological variables of relative humidity over ice

Table 5. Meteorological variables and their alternatives needed to calculate aCCFs.

Meteorological variables	*Alternatives*
Potential vorticity unit $[10^{-6}Kkg^{-1}m^2s^{-1}]$	Temperature $[K]$, components of wind $[ms^{-1}]$
Relative humidity $[\%]$	Specific humidity $[kgkg^{-1}]$
Outgoing longwave radiation (OLR) $[Wm^{-2}]$	Top net thermal radiation (ttr) $[Jm^{-2}]$
Incoming solar radiation at top of the atmosphere $[Wm^{-2}]$	Date, declination angle
Temperature $[K]$	
Geopotential $[m^2s^{-2}]$	

and temperature, has to be fulfilled. SAC describes the formation of both short-lived and long-lasting (or persistent) contrails. For the persistence of contrails a second criteria is needed: the ambient air has to be supersaturated with respect to ice, meaning

285 that the relative humidity over ice ($rhum_{ice}$) is higher that 100%. Within CLIMaCCF the PCFA are calculated in the processing step. Here the user has two possibilities: The first possibility is to calculate PCFA by using the thresholds, one for the temperature ($T < 235K$) and one for the relative humidity over ice (>100%) (see supplement Yin et al., 2022) (PCFA-ISSR). The second possibility, which is more accurate, as it takes into account aircraft/engine properties, is to use SAC to define the thresholds and additionally assume ice supersaturation (PCFA-SAC).

290 The **calculation of the individual and merged aCCFs** within CLIMaCCF is based on the aCCF formulas of Yin et al. (2022) (see Appendix A). By using the provided original and preprocessed input data the individual and merged aCCFs are calculated. Moreover user specific conversion factors due to the selected physical climate metric, efficacy, and aircraft specific emission indices are needed. Table 6 summarizes all the individual aCCFs and parameters needed to calculate merged aCCFs. Additionally the processing block includes the **calculation of climate hotspots**, areas that are very sensitive to aviation emission. The

295 calculation of climate hotspots is based on the calculated merged aCCFs. For identifying these climate hotspots a threshold based on the merged aCCFs is needed. This threshold can either be fixed to a user defined parameter or it can be determined dynamically within CLIMaCCF by calculating the percentile value (e.g. 90% or 95%) of the merged aCCF (a more detailed explanation of the dynamical approach is given in Section 4).

3.3 Output block

300 In the output block (lower right box in Fig. 1), the processed aCCFs are saved. In the current version, for saving aCCFs (e.g., individual aCCFs, merged aCCF, and climate hotspots) and weather variables (if selected), netCDF and PICKLE file formats can be selected. In addition, the user can choose the GeoJSON format for storing polygons of climate sensitive regions (i.e., climate hotspots).

Table 6. The functions and variables needed to calculate merged aCCFs.

Function	Unit	Physical input parameter	Range
$aCCF_{O3}$	K/kg(NO$_2$)	Geopotential, temperature	≥ 0 (warming)
$aCCF_{CH4}$	K/kg(NO$_2$)	Geopotential, solar radiation	≤ 0 (cooling)
$aCCF_{H2O}$	K/kg(fuel)	Potential vorticity unit	≥ 0 (warming)
$aCCF_{contrail-day}$	K/km	Outgoing longwave radiation, relative humidity, temperature	$-10^{-10} \leq$ aCCF$_{\text{contrail-day}} \leq 10^{10}$ (cooling/warming)
$aCCF_{contrail-night}$	K/km	Temperature, relative humidity	aCCF$_{\text{contrail-night}} \geq 0$ (warming)
EI$_{NOx}$	g(NO$_2$)/kg(fuel)	Aircraft/engine	EI$_{NOx} \geq 0$
F_{km}	km/kg(fuel)	Aircraft/engine	$F_{km} \geq 0$
PCFA	-	threshold for relative humidity over ice and temperature, aircraft/engine properties	PCFA = [0, 1]

4 Application of CLIMaCCF to ERA5 reanalysis data

305   The Python Library CLIMaCCF allows to easily generate output of spatially and temporal resolved climate impact of aviation emissions by using available aCCFs. As mentioned above the individual aCCFs of NO$_x$ induced ozone and methane, water vapour, contrail-cirrus, and the merged non-CO$_2$ aCCFs can be calculated with CLIMaCCF. In this Section we describe different characteristic patterns of individual and merged aCCFs over the European airspace. We also compare merged aCCFs using different assumptions of aircraft types and metrics, and we explain how to identify regions that are very sensitive to aviation

310   emissions (so called climate hotspots) and how these climate hotspots behave.

The meteorological input data, used for calculating the aCCFs within the CLIMaCCF were taken from the ERA5 high resolution realisation reanalysis data set (Dee et al., 2011). ERA5 is the fifth generation of the European Centre for Medium-Range Weather Forecasts (ECWMF) atmospheric reanalysis. ERA5 high resolution (HRES) data are archived with a horizontal resolution of 0.28°x 0.28°.

4.1 Analysis of individual and merged aCCFs by using the Python Library CLIMaCCF

315

In this subsection we show typical patterns of water vapour, NO$_x$-induced (including ozone, methane and PMO), contrail-cirrus and merged non-CO$_2$ aCCFs at 12 UTC (under day-time conditions) on 15 June, 2018, over the geographical region of Europe (15°W-30°E, 35°-60°N) at a pressure level of 250 hPa as an example. With this analysis we aim to give an impression of the typical structure and of gradients of the specific aCCFs over the European airspace. Note that in this subsection we generated

320   individual and merged aCCF using aCCF-V1.1 and by assuming the climate metric of F-ATR20 with inclusion of efficacies. For merging we used typical transatlantic fleet mean parameters (see Section 2). In case of merged aCCFs we will focus on the merged non-CO$_2$ aCCFs (Eq. 1), as the merged aCCF pattern doesn't change if including the CO$_2$ aCCF which is as constant

value in time and location. But of course, that for climate optimal trajectory optimization, fuel consumption has to be also taken into account, as this is directly linked to CO_2 emissions.

325 ### 4.1.1 Water vapor aCCF

Fig. 2 presents the typical water vapour aCCFs over Europe for the specific summer day. As aircraft induced water vapour emissions have a warming effect, the water vapour aCCFs reveal positive values in all regions. The values of water vapour aCCF are highly variable, and they vary with locations by a factor of about three. This regional variation in the aCCFs pattern highly follows the weather pattern; the maximum value can be observed over the region with negative geopotential height
330 anomalies (see overlaid green lines), indicating a low precursor and low tropopause.
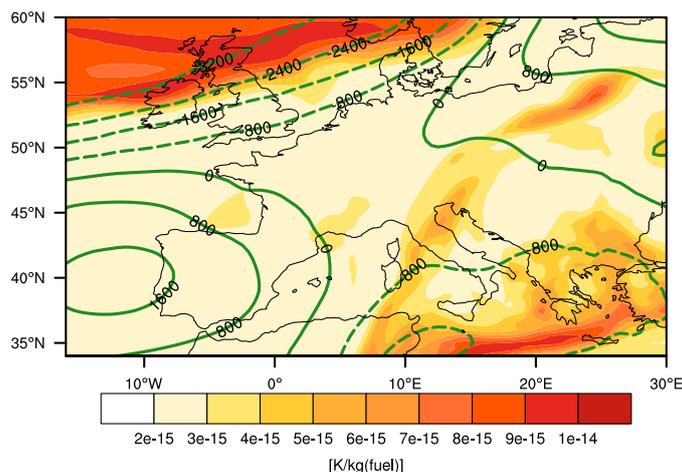
Figure 2. Water vapour aCCF at pressure level of 250 hPa over Europe at 12 UTC on 15 June, 2018. Units are given in [K/kg(fuel)]. Overlaid green lines indicate positive (solid line) and negative (dashed line) geopotential height anomalies (in m²/s²).

4.1.2 NO$_x$ induced aCCFs

To better understand the total NO$_x$ induced aCCF, the NO$_x$ aCCF is displayed in Fig. 3 together with the ozone and methane aCCF. Note that the long-term primary mode ozone PMO, is included here in the methane aCCF. The ozone aCCF (Fig. 3a) is positive (warming), as NO$_x$ emissions from aviation induce the production of the greenhouse gas ozone. It reveals generally
335 higher values in southern regions, as the photochemical ozone formation increases with the availability of sunlight as well as with temperature. Additionally, the synoptical weather pattern influences the ozone aCCF values, as emitted NO$_x$ that is transported to lower latitudes experiences more solar radiation, and thus photochemical ozone production is higher compared to that which remains at higher latitudes. The methane aCCF is negative (Fig. 3b), as NO$_x$ emissions cause a decrease in methane concentrations, as there is a decrease in warming from methane. The resulting total NO$_x$ aCCF (Fig. 3c), a combination of
340 ozone warming and methane net cooling effects, reveals that the ozone effect dominates the overall warming effect of NO$_x$

emissions. Note that by using the metric of ATR20 and an underlying future emission scenario, the differences in lifetime between NO_x, ozone and methane are taken into account.
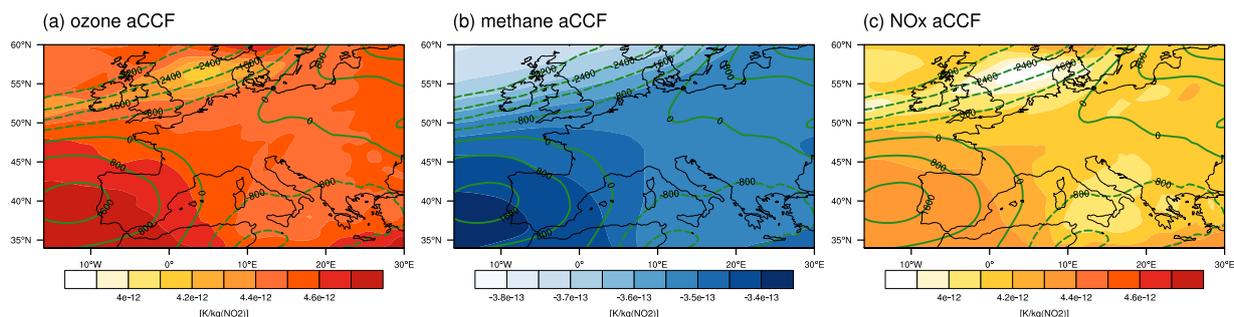

Figure 3. (a) Ozone aCCF, (b) methane aCCF (including PMO) and (c) total NO_x aCCF (sum of ozone, methane and PMO aCCFs) at pressure level 250 hPa over Europe at 12 UTC on 15 June, 2018. Units are given in [K/kg(NO_2)]. Overlaid green lines indicate positive (solid line) and negative (dashed line) geopotential height anomalies (in m^2/s^2).

4.1.3 Contrail-cirrus aCCFs

Only if the atmospheric conditions allow for a contrail formation, the contrail aCCF is non-zero. Fig. 4 shows the day-time
345 contrail-cirrus aCCF that can lead to either a positive or negative climate impact. Whether the climate impact is positive or negative depends mainly on the solar insolation, as contrails not only reduce the outgoing longwave radiation (warming) but also reflect the shortwave incoming radiation (cooling). The spatial variability in the contrail aCCF is very high and ranges from zero (regions with no persistent contrail formation) to high positive or negative values. This is clear as the formation of persistent contrails is highly sensitive to the actual atmospheric conditions.
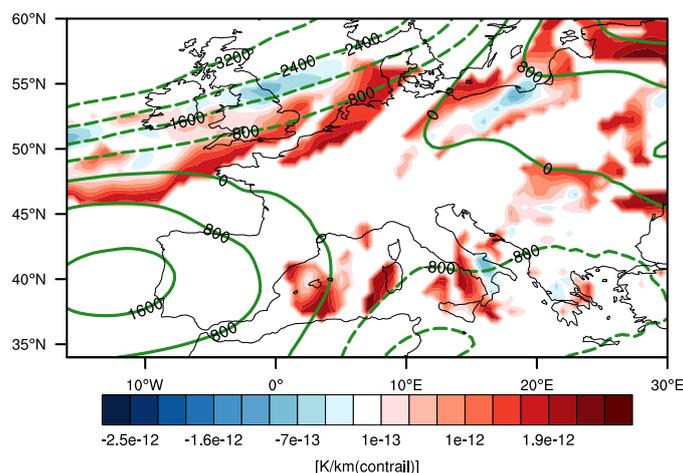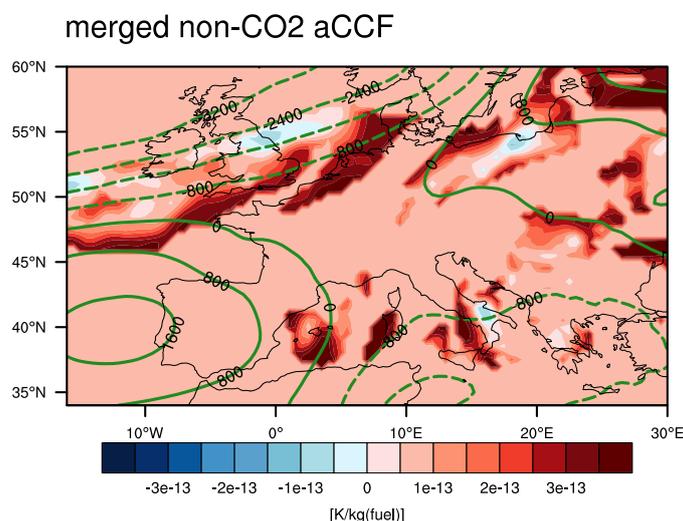
Figure 4. Day-time contrail aCCF at pressure level 250 hPa over Europe at 12 UTC on 15 June, 2018. Units are given in [K/km(contrail)]. Overlaid green lines indicate positive (solid line) and negative (dashed line) geopotential height anomalies (in m^2/s^2).

4.1.4 Merged non-CO$_2$ aCCFs

Figure 5 finally shows the merged non-CO$_2$ aCCF, which combines the water vapour, NO$_x$-induced and contrail-cirrus aCCFs. The shown merged aCCF is calculated based on the climate metric of F-ATR20, taking into account the different efficacies of contrails, ozone and methane. Moreover the typical averaged fleet mean values of transatlantic flights are taken for the NO$_x$ emission index and the specific range. The comparison of the individual aCCF components (see Figs. 2-4) with the merged non-CO$_2$ aCCF (Fig. 5) clearly shows that the contrail-cirrus aCCF dominates the non-CO$_2$ climate impact in the regions where contrails form. By converting all the individual aCCFs to the same unit of K/kg(fuel), the direct comparison of the aCCFs can be allowed (see Appendix B, Figure A2 first row). This shows that contrail aCCF have the highest climate impact in the contrail formation areas, followed by the NO$_x$-induced aCCF; whereas the water vapour aCCF is of negligible magnitude in this case. Thus, adding the high values of positive contrail aCCF to the smaller positive NO$_x$ aCCF values leads to very high values in the merged aCCF, whereas areas of negative contrail aCCF mostly lead to the negative merged aCCF, as the magnitude of the negative aCCF is often higher than that of the NO$_x$-induced aCCF. On the basis of the merged aCCF (Fig. 5), a hypothetical climate-optimized European flight (which will stay on this pressure level for simplification) would certainly try to avoid the areas with high positive merged aCCFs. Further, this flight trajectory will probably find a compromise between avoiding long distances through enhanced climate warming areas and at the same time avoiding long detours as these would induce a penalty with respect to CO$_2$ aCCF. Thus if the trajectory is optimized based on the merged non-CO$_2$ aCCF this penalty is not taken into account.

Figure 5. Merged non-CO$_2$ aCCF at pressure level 250 hPa over Europe at 12 UTC on 15 June, 2018. Units are given in [K/kg(fuel)]. Overlaid green lines indicate positive (solid line) and negative (dashed line) geopotential height anomalies (in m^2/s^2).

4.2 Sensitivity of merged aCCFs to different aircraft/aircraft classes and climate metrics

As mentioned above, the merged aCCFs can be used as advanced MET information for flight planning, as CLIMaCCF enables quantifying the total non-CO$_2$ climate impact as four-dimensional data set (latitude, longitude, altitude and time), that is neces-

370   sary for a climate optimized trajectory. In Section 4.1, we showed the merged aCCF constructed with CLIMaCCF assuming the climate metric of F-ATR20 (the efficacies included) and the transatlantic fleet mean value of the NO$_x$ emission index and the specific range. However, as described in Section 2, there are several choices for generating the merged aCCFs. These choices are related to the climate objective (climate metric) and the emission behaviour of the aircraft type and depend of course on a user objective. In the following we investigate how sensitive the merged non-CO$_2$ aCCFs are to different assumptions. Table

375   7 summarizes the different considerations of merged non-CO$_2$ aCCFs that were performed with CLIMaCCF. The reference calculation is the same as shown in Section 4.1 (using the climate metric F-ATR20, inclusion of efficacies, and emission indices of typical fleet mean values of transatlantic flights). Additionally we conducted three sensitivity calculations with height dependent emission indices and specific ranges of different aircraft types (i.e. regional, single-aisle and wide-body); and one sensitivity calculation with a different climate metric of F-ATR100.

380   In the first three sensitivity calculations (SENS-AC1, SENS-AC2 and SENS-AC3), we varied the emission indices by using different aircraft types. With choosing different aggregated aircraft types (i.e. regional, single-aisle and wide-body), the respective values of F$_{km}$ and EI_{NOx} were used (see Tables 1 and 2). Note moreover that, in contrast to the mean fleet value used for the reference calculation, EI_{NOx} and specific range values are flight altitude dependent. These sensitivity calculations are used to investigate how the aircraft type influences the overall climate impact in terms of the average temperature change. Figure 6

385   shows the merged aCCFs for the reference calculation (REF) and for the aircraft dependent sensitivity calculations (SENS-

Table 7. Overview on the conducted calculations of merged non-CO_2 aCCFs. Besides the reference calculation (REF), which uses transatlantic fleet mean values, there are three sensitivity calculations using height dependent aircraft/engine parameters (i.e. EI_{NOx}, F_{km}) of different aggregated aircraft types (SENS-AC1, SENS-AC2 and SENS-AC3) and one sensitivity calculation using a different climate metric (SENS-M1). Efficacy is is taken into account for all simulations.

	REF	SENS-AC1	SENS-AC2	SENS-AC3	SENS-M1
climate metric	F-ATR20	F-ATR20	F-ATR20	F-ATR20	F-ATR100
aircraft/engine class	fleet mean	regional	single-aisle	wide-body	fleet mean

AC1, SENS-AC2 and SENS-AC3) on 15 June, 2018 at a pressure level of 250 hPa. Additional Figure A1 of the Appendix B provides aircraft/engine dependent merged aCCF patterns together with the respective water vapour, NO_x and contrail-cirrus aCCFs, all given in the same unit of K/kg(fuel). Generally, for all aggregated aircraft types the highest climate impact is found in the areas of contrail formations. Comparing the aircraft type dependent merged aCCFs reveals that contrails are more dom-

390   inant for the regional and single-aisle aircraft types. In the case of regional (SENS-AC1) and single-aisle (SENS-AC2) aircraft types, the merged aCCFs have very high contrail aCCF values (see Fig. A1), leading to the high absolute merged aCCF values. The maximum merged aCCF values are smaller if the transatlantic fleet mean (REF) and the wide-body (SENS-AC3) aircraft type emission indices are chosen. Moreover, in regions where no contrails form, the NO_x-induced aCCF (i.e. the sum of the ozone, methane and PMO aCCFs) shows relative high values for REF and SENS-AC3, compared to those for SENS-AC1 and

395   SENS-AC2. Comparing to the aircraft/engine dependent NO_x emission indices and flown distances at flight altitude of 35000 ft (roughly corresponding to the pressure layer of 250 hPa) in Tab. 1 and Tab. 2, these differences can be explained: at this cruise altitude the aggregated regional aircraft type shows the lowest EI_{NOx} (7.968 g(NO_2/kg(fuel))), but the highest flown distance values F_{km} (0.488 km/kg(fuel)).
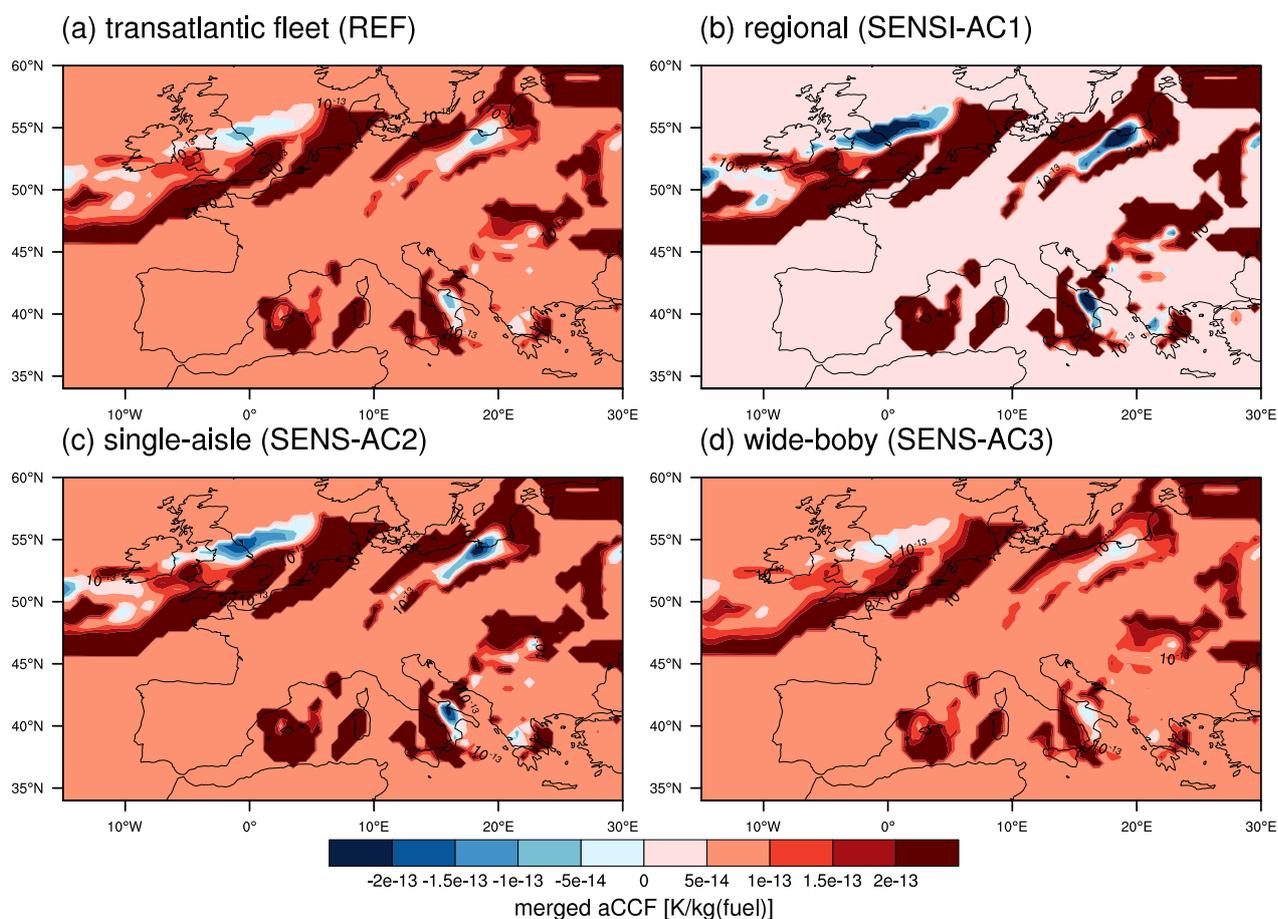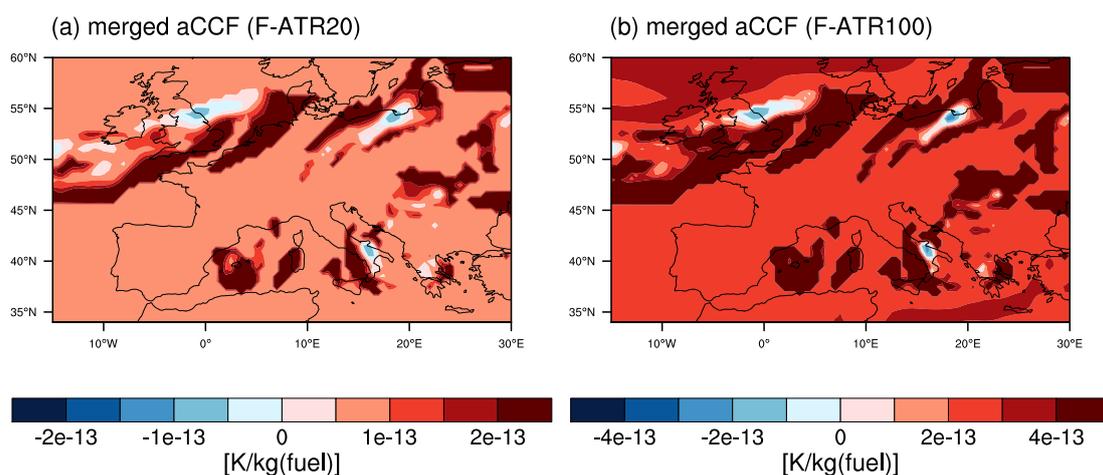
Figure 6. Merged non-CO_2 aCCF at pressure level 250 hPa over Europe on 15th of June 2018 (12 UTC), using four different assumptions for the NO_x emission index and the flown distance values: (a) typical transatlantic fleet mean, (b) regional aircraft type, (c) single-aisle aircraft type and (d) wide-body aircraft type. Units are all given in [K/kg(fuel)].

To generate a merged non-CO_2 aCCF, it is necessary to choose a consistent climate metric for all individual aCCFs. As mentioned in Section 2.4, there are many metrics used in literature to assess the climate impact; however the choice of the metric depends on the objective of the study (e.g. Grewe and Dahlmann, 2015). CLIMaCCF provides the possibility to choose between a set of different climate metrics. Thus, we can show how different metrics influence the merged non-CO_2 aCCF. As example we here compare the reference calculation (REF), which is based on F-ATR20 (Fig.7a) to the SENS-M1 calculation, which assumes the climate metric of F-ATR100 (Fig. 7b). For the F-ATR100 metric, the focus lies more on long-term mitigation effects, whereas the choice of F-ATR20 metric focuses on the short-term mitigation effect. Choosing the time horizon of 100

years for the F-ATR largely impact the absolute values of the merged aCCF, as the metric conversion factor of all species is higher for F-ATR100 (see Tab. 3). Moreover, in Fig. A2 (Appendix B) the individual aCCFs for these two metrics are shown in terms of the same unit of K/kg(fuel) and we see that the climate impact of NO_x-induced emissions gets somehow more important compared to the contrail aCCFs in case of ATR100.

Figure 7. Merged non-CO_2 aCCF at pressure level 250 hPa over Europe at 12 UTC on 15th June, 2018, using two different assumptions for the climate metric: (a) F-ATR20 (REF) and (b) F-ATR100 (SENS-M1).

4.3 Identification of climate sensitive regions (climate hotspots)

Any trajectory planning tool capable to plan climate-optimized aircraft trajectories (see Simorgh et al. (2022)), can use the information of the location, altitude and time dependent climate impact of non-CO_2 emissions and aim to avoid such highly sensitive regions by planning for an alternative, climate-optimized or eco-efficient aircraft trajectory. CLIMaCCF offers the possibility to identify those regions with large climate impact, called climate hotspots. Threshold values, that define these climate hotspots, have to be provided. These threshold values are based on the merged non-CO_2 aCCF values: if the merged

aCCF exceeds a certain threshold value of the merged aCCF the region is defined as climate hotspot. As the merged aCCFs highly vary with season, flight altitude, geographical latitude, day- and night-time condition and synoptic weather situation, these threshold values should be determined dynamically for every time step and flight altitude over a certain geographical region (e.g. European airspace). To do so, we calculate the percentile (e.g. 95% percentile) of the merged aCCF distribution

420 over all grid-points spanning e.g. the European airspace (in our example we use the geographical region of 35°-60°N, 15°W-30°E). This percentile then provides the time step and level dependent threshold of the merged aCCF. As mentioned above, regions are defined as climate hotspots if the corresponding merged aCCF lies above this threshold. Thus, e.g. in case of the 95% percentile the highest 5% of the merged aCCF are declared as climate hotspots. In CLIMaCCF the user has the possibility to select the geographical region over which the percentile of the merged aCCF is calculated as well as the percentage (e.g.

425 90%, 95%) of the percentile.

Figure 8 illustrates such climate hotspots (in red) over the European airspace for the different cruise altitudes of 200, 250 and 300 hPa exemplary for the 15th June 2018 at 12 UTC. The underlying merged non-CO_2 aCCF used here is based on the REF calculation (see Tab. 7 and Fig. 5). By selecting the 95% percentile for the calculations we get different threshold values for different altitudes: $2.945e^{-13}$ K/kg(fuel) for 200 hPa, $3.256e^{-13}$ K/kg(fuel) for 250 hPa and $2.687e^{-13}$ K/kg(fuel) for 300

430 hPa. The threshold at 250 hPa has the highest value, meaning that aviation's climate impact (in terms of merged non-CO_2 aCCFs) is generally larger here. Comparing the climate hotspot patterns in Figure 8 it is clear that these regions vary a lot for different altitudes.
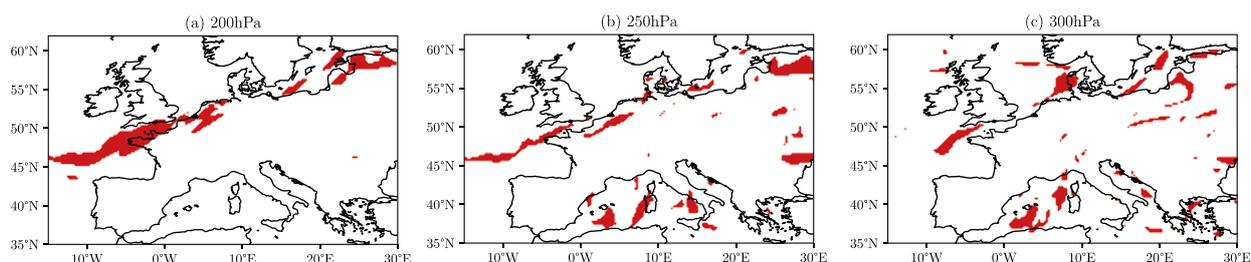
Figure 8. Climate hotspots over the European airspace on the 15th of June 2018 (12 UTC) for the flight altitudes (a) 200 hPa, (b) 250 hPa and (c) 300 hPa. The thresholds are based on the respective (pressure level dependent) 95% percentile of the merged non-CO_2 aCCF.

5 Discussion

435 ### 5.1 CLIMaCCF configuration

With the open source Python Library CLIMaCCF we provide a simple and easy to use framework for quantifying the spatially and temporally resolved climate impact of aviation emissions by making use of the aCCFs that are published in the studies of van Manen and Grewe (2019); Yamashita et al. (2020); Yin et al. (2022) and Matthes et al. (2022, in preparation). CLIMaCCF

is easy to install and to run and it efficiently calculates the individual and merged non-CO_2 aCCFs, taking the actual meteo-
rological situation into account. Merged non-CO_2 aCCFs are generated by combining the individual aCCFs of water vapour,
NO_x- induced ozone and methane and contrail cirrus by taking assumptions on the technical specification of the engine/aircraft
combination (i.e. EI_{NOx} and F_{km}), and on an appropriate physical climate metric. With this newly developed Python Library
the user has got the possibility to investigate merged aCCFs for three different aggregated aircraft types (regional, single aisle,
wide-body) that provide flight level dependent values of EI_{NOx} and F_{km} (for details see Table 1 and 2). This novel feature of
calculating merged aCCFs by considering the flight level and aircraft dependent values of EI_{NOx} and F_{km}, rather then using
the transatlantic fleet mean values, leads to a better representation of aviation's non-CO_2 climate impact. Compared to the
study of Frömming et al. (2021), which showed aviation's merged climate impact (in terms of CCFs) by using transatlantic
fleet mean values, this is a real improvement, as merged aCCFs vary significantly for different aircraft types as also shown in
Fig. 6.

Moreover CLIMaCCF offers the possibility to calculate aCCFs for a set of different physical climate metrics. For instance the
user has the flexibility to calculate the aCCFs for the climate metric of global average temperature response (ATR) with pulse
emission or future emission scenario over the time horizons of 20, 50 and 100 years. However we want to point out here, that
any optimization study has to carefully choose an adequate physical climate metric (i.e. its climate indicator, emission scenario
and time horizon), so that it is suitable to the specific application, that depends on taken strategic decisions, on given constraints
and on policy assumptions (e.g. Fuglestvedt et al., 2010; Grewe and Dahlmann, 2015). For example a pulse emission compares
the future climate impact in a given year, whereas a future emission scenario compares the effect of increasing emissions over
a future time period. This leads to different estimates of the ATR, as also shown in Fig. 7.

5.2 Threshold of relative humidity for ice supersaturated regions (ISSR)

Besides the wise selection of an appropriate climate metric, also other configuration parameters have to be chosen carefully
by the user. Thus, if using the Python Library CLIMaCCF for calculating the climate impact of contrails the user has to pay
special attention when defining the threshold of relative humidity for ice supersaturated regions (ISSR). In case of contrail
aCCFs we need to determine these ISSRs, as only in these regions persistent contrails can form. And only for these regions the
contrail aCCF is calculated. These ISSRs are identified by two conditions. The temperature is below 235 K (in order to avoid
identification of mixed-phase regions (Pruppacher et al., 1998)) and the relative humidity with respect to ice (RH_{ice}) exceeds
100% (see e.g. Yin et al. (2022), their supplement on contrail aCCF). However, for considering the sub-grid-scale variability
in the relative humidity field in numerical weather forecast model data, e.g. ERA5, RH_{ice} thresholds below 100% are needed.
For example Irvine et al. (2014) showed that the relatively coarse resolution of the ERA-Interim data, leads to a grid box with
a grid mean humidity slightly below 100%, as it is likely within this grid box that some air parcels show relative humidity
values above 100%. In the following we explain how we derive the threshold value of RH_{ice} in order to consider the sub-grid-
scale variability for the data product ERA5 HRES (see Section 4). To do so we calculated the annual mean (2009-2010) ISSR
frequency over the European region (5°W- 30°E, 40°N-60°N) using the ERA-5 data set. For the ISSR frequency calculation

we varied the threshold value of RH$_{ice}$ (i.e. taking 90% and 95%), but leaving the temperature threshold of 235 K constant and compared the results to the observational based ISSR frequency values of the study of Petzold et al. (2020). This study

475   used in-situ measurement data of temperature and RH$_{ice}$ from the full MOZAIC program[1] over the period 1995-2010. Table 8 summarises the results of our ERA-5 based ISSR calculations together with the results of Petzold et al. (2020) obtained by observational data. The frequency of ISSR in the European area is shown for three different vertical levels, the tropopause layer (TPL, thermal tropopause), the upper troposphere (UT, 30 hPa below thermal tropopause), and the lower stratosphere (LS, 30 hPa above thermal tropopause). From this table we see that by setting the RH$_{ice}$ threshold value to 90% for ERA5 the ISSR

480   values of Petzold et al. (2020) are best matched. Thus, taking RH$_{ice}$ threshold values of 90% the ISSR frequency of Petzold et al. (2020) is only slightly overestimated in the TPL (2%) and in the UT (1%). Note, that the threshold value for the RH$_{ice}$ have tobe adopted if using other resolutions of ERA-5 data or other data products. The contrail aCCF shown in Section 4 of this publication uses the 90% threshold, as it is based on ERA-5 HRES input data.

Table 8. Frequency/Coverage area of annual mean ISSR (in %) over the European region (5°W- 30°E, 40°N-60°N) at the TPL, LS (30 hPa above thermal tropopause), UT (30 below thermal tropopause). Values are shown for MOZAIC in-situ measurement data Petzold et al. (2020) and for ERA-5 HRES using RH$_{ice}$ thresholds of 90% and 95%,

	Petzold et al. (2020)	RH$_{ice}$=90%	RH$_{ice}$=95%
TPL	18.8%	20.55%	16.7%
LS(TPL-30 hPa)	1.6%	0.65%	0.4%
UT(TPL+30 hpA)	30.95%	31.85	26.75%

5.3   Limitations of prototype aCCFs

485   It is also essential to note here that CLIMaCCF is facing limitations. An important limitation is the prototype character of the aCCFs. As described in Section 2.1 the aCCF algorithms were developed based on a set of detailed comprehensive climate model simulations for meteorological summer and winter conditions with focus on the North Atlantic flight corridor (van Manen and Grewe, 2019; Frömming et al., 2021). We do not recommend a off-design use of these aCCFs, especially using the aCCFs for tropical regions or for spring and autumn seasons. However the development of the aCCFs is current research

490   activity and an expansion of their geographic scope and seasonal representation is ongoing. New developments and improved understanding in aCCF algorithms will provide updated aCCF formulas that will be included to future versions of CLIMaCCF, as soon as they are published. As the current version of CLIMaCCF provides the possibility to chose between different aCCF versions, it will be easy to implement further aCCF versions.

Moreover aCCFs are associated with different aspects of uncertainties, as current scientific understanding still recognizes

495   uncertainties in the quantitative estimates of weather forecast and climate impact prediction. The uncertainty range of the indi-

---

[1]The MOZAIC (Measurement of Ozone, Water Vapour, Carbon Monoxide and Nitrogen Oxides by Airbus In-Service Aircraft) program was designed to collect trace gases by using automatic equipment installed on board of five long-range Airbus A340 operated by European airlines. See Marenco et al. (1998)

vidual aviation climate effects was recently specified in Lee et al. (2021). They showed that still large uncertainties of individual non-CO_2 effects (i.e. contrail-cirrus, NO_x, water vapour as well as the indirect aerosol effect) estimates exist. Within the EU project FlyATM4E a concept is developed that incorporates these uncertainties in order to generate robust aCCFs (Matthes et al., 2022, in preparation). Thus for this purpose educated guess estimates of aCCF were developed (aCCF-V1.1, Matthes et al. (2022, in preparation)) in order to shift the aCCFs quantity to state-of-the-art research. These educated guess aCCF are included in CLIMaCCF and can be selected in the configuration script. A more detailed description on these educated guess aCCFs, that are basically aCCFs that are multiplied with educated guess factors, is given in Matthes et al. (2022, in preparation). Besides choosing between two different aCCF versions (i.e aCCF-V1.0, aCCF-V1.1), the individual aCCFs (either Version 1.0 or Version 1.1) can be modified by multiplied by any factors specified by the user. By using these alternative factors the user has the possibility to generate upper and lower limit estimates of the aCCF. With that the different degrees of level of scientific understanding can be reflected.

5.4 Application using ERA5 reanalysis data

CLIMaCCF was successfully applied to ERA5 HRES reanalysis data. Obtained results show the characteristic patterns of the individual and merged aCCFs for a single day in June 2018 over the European airspace. The aCCFs patterns of the individual aCCFs show the overall positive climate impact of NO_x and water vapour emissions and negative and positive values for the daytime contrail aCCFs. These features were found in several studies before (e.g. Frömming et al. (2021); Yamashita et al. (2021); Yin et al. (2022)). Looking at the merged aCCFs it is clear, that NO_x and contrail aCCF are dominating the magnitude of merged aCCFs, while water vapour aCCF only plays a minor role for the total non-CO_2 aCCF. Overall the merged aCCF pattern is highly dominated by the very variable contrail aCCF pattern and thus avoiding the contrail climate impact leads to the most promising mitigation potential. This is in line with earlier studies, that also showed the dominating effect of contrail-cirrus (e.g. Frömming et al., 2021; Yin et al., 2022; Castino et al., 2021).

6 Conclusions

In this publication we developed a tool for efficiently calculating the spatially and temporally resolved climate impact of aviation emission by making use of the aCCFs. In the novel Python Library CLIMaCCF, these aCCFs can be simply calculated with meteorological input data from the forecast or reanalysis data products of ECWMF. Besides the individual aCCFs of water vapour, nitrogen oxide (NO_x) induced ozone and methane and contrail-cirrus aCCF, CLIMaCCF generates merged (non-CO_2) aCCFs that combine the individual spatially and temporally resolved aCCFs. However, these merged aCCFs can be only constructed with the technical specification of the EI_{NOx} and F_{km} of a selected engine/aircraft type. Additionally, these merged aCCFs can be calculated for a range of user-defined parameters, as e.g. the choice of a physical climate metric. Thus, generating user defined merged non-CO_2 aCCFs can serve as advanced MET info for trajectory flight planning. Additionally CLIMaCCF provides a method to identify regions that are very sensitive to aviation emissions.

We apply CLIMaCCF to the ERA5 HRES reanalysis data set and show the characteristic pattern of the individual and merged aCCFs for a single day in June 2018 over the European airspace. Our results describe the geographical distributions of indi-
530 vidual and merged non-CO_2 aCCFs. By comparing the individual aCCFs to the merged aCCF shows that contrail aCCFs are dominating the total non-CO_2 impact. These merged aCCFs were calculated for different aircraft/engine combinations and with different metrics, showing that magnitude and structure of merged aCCFs vary with different assumption for aircraft/engine combination or for climate metric.

Current limitations of CLIMaCCF could be addressed in future development. Overall future efforts should be directed towards
535 improvement of aCCFs and expansion of user configuration parameters. Thus possible future extensions of CLIMaCCF could for example include the adaption of the source code to other data products (rather than only ECMWF data products), as e.g. climate chemistry model data or other numerical weather forecast data. Additionally future versions of CLIMaCCF could include metric conversion factors for a larger set of climate metrics, as e.g. greenhouse warming potential. Also an expansion of the emission indices to further engine/aircraft combinations or to future aircraft types is possible.
540 Thus overall, with CLIMaCCF we provide a user friendly tool, that can be used for climate optimized trajectory planning.

Code availability. CLIMaCCF is a newly developed open source Python Library. It is developed at https://github.com/dlr-pa/climaccf/ and is available via the DOI (https://doi.org/10.5281/zenodo.6977272). It is distributed under the GNU Lesser General Public Licence (Version 3.0). The respective User Manual, which includes details on the software and its user configuration is included as supplement of this paper.

Data availability. The ERA5 data sets used in this study can be freely accessed from the respective repositories after registration. ERA5
545 data were retrieved from the Copernicus Climate Data Store (https://cds.climate.copernicus.eu/, European Reanalysis 5, 2020). Last access:05/2022.

Appendix A: Mathematical formulation of aCCFs-V1.0

A detailed explanation of the aCCFs approach can be found in van Manen and Grewe (2019) for NO_x induced species and water vapour, and in the case of the contrail aCCFs approach, a detailed description is given in (Yin et al., 2022). In the following
550 we describe the mathematical formulation of the individual aCCFs (aCCF-V1.0, see Yin et al. (2022)). We want to mention here that the aCCF-V1.0 (Yin et al., 2022) are not identically to van Manen and Grewe (2019), but differ by certain factors (explanation is given in Yin et al. (2022)). Note moreover that all aCCF formulations are consistently given in P-ATR20, and efficacy is excluded.

NO_x induced aCCFs
555 The total NO_x aCCFs is a combined effect of the NO_x induced ozone aCCFs and the NO_x induced methane aCCFs. This can be explained by the fact that the NO_x emissions of aviation lead to the formation of ozone (O_3) which induces a warming of the atmosphere. Additionally, NO_x emissions lead to the destruction of the long lived GHG methane (CH_4) which then induces

a cooling of the atmosphere. In the following, the mathematical formulation of both the ozone and the methane aCCFs are described.

NO_x induced ozone aCCFs

The mathematical formulation of the ozone aCCFs is based on temperature T [K] and geopotential Φ $[m^2/s^2]$. The relation for the ozone aCCFs (aCCF$_{O3}$) at a specific atmospheric location and time is given in temperature change per emitted NO_2 emission [K/kg(NO_2)]:

$$aCCF_{O3} = \begin{cases} -2.64*10^{-11} + 1.17*10^{-13}*T + 2.46*10^{-16}*\Phi - 1.04*10^{-18}*T*\Phi, & \text{if } aCCF_{O3} \geq 0. \\ 0, & \text{if } aCCF_{O3} < 0 \end{cases} \quad \text{(A1)}$$

Accordingly, the ozone aCCFs takes positive values, and is set to 0 in case of negative aCCF values.

NO_x induced methane aCCFs

The methane aCCFs is based on the geopotential Φ $[m^2/s^2]$ and the incoming solar radiation at the top of the atmosphere F$_i n$ $[W/m^2]$. The relation of the methane aCCFs (aCCF$_{CH4}$) at a specific location and time is given in temperature change per emitted NO_2 emission[K/kg(NO_2)]:

$$aCCF_{CH4}(\Phi, F_{in}) = \begin{cases} -4.84*10^{-13} + 9.79*10^{-19}*\Phi - 3.11*10^{-16}*F_{in} + 3.01*10^{-21}*\Phi*F_{in}, & \text{if } aCCF_{CH4} < 0 \\ 0, & \text{if } aCCF_{CH4} > 0 \end{cases}$$

$$\text{(A2)}$$

Thus, the methane aCCFs is negatively defined. It is set to 0 if the term aCCF$_{CH4}$ is 0 or positive. F$_i n$ is defined as incoming solar radiation at the top of the atmosphere as a maximum value over all longitudes and is calculated by: $F_{in} = S*cos\theta$, with total solar irradiance S=1360 Wm^{-2} , $cos\theta = sin(\phi)sin(d) + cos(\phi)cos(d)$ and $d = -23.44° * cos(360°/365° * (N + 10))$. Here θ is the solar zenith angle, ϕ is latitude, and d is the declination angle, which defines the time of year via the day of the year N.

The mathematical formulation of the ozone aCCF is only valid for the short-term ozone effect of NO_x. The primary mode ozone (PMO), which describes the long-term decrease in the background ozone, as result of a methane decrease, is not included (van Manen and Grewe, 2019). Also, the stratospheric water vapour decrease via the methane oxidation is not included. Thus, if merging total NO_x effect be aware that only the NO_x effect on short term ozone increase and on methane decrease is taken into account. For NO_x induced PMO climate impact we have the possibility to include it to the total NO_x aCCF, as the PMO aCCF can be derived by applying a constant factor of 0.29 to the methane aCCF (Dahlmann et al., 2016). Thus $aCCF_{PMO} = 0.29 * aCCF_{CH4}$.

Water vapour aCCFs

The water vapour aCCFs is based on the Potential Vorticity (PV) given in standard PV units $[10^{-6}Kkg^{-1}m^2s^{-1}]$. Following the relation of the water vapour aCCFs (aCCF$_{H20}$) at a specific location and time is given in temperature change per fuel

[K/kg(fuel)]:

580 $$aCCF_{H20}(PV) = 2.11 * 10^{-16} + 7.70 * 10^{-17} * |PV| \qquad (A3)$$

The absolute value of the PV is taken to enable a calculation on the southern hemisphere, where PV has a negative sign.

Contrail aCCFs

The algorithm that generates contrail aCCFs is obtained by the calculation of the contrail radiative forcing, using ERA-Interim

585 data as input (Yin et al., 2022). In contrast, the above described NO_x and water vapour aCCFs are based on CCFs that were calculated with the chemistry climate model EMAC (Jöckel et al., 2016). Contrail aCCFs are calculated separately for day-time and night-time contrails, because their climate impact differs between daylight and darkness, as the shortwave forcing is only relevant for daylight conditions. To differ between day-time and night-time contrail aCCFs, the local time and solar zenith angle are calculated. For locations in darkness, the time of sunrise is calculated. If the time between the local time and sunrise

590 is greater than 6 h, the night-time contrail aCCFs is applied. In order to determine the contrail aCCFs, the RF of day-time or night-time contrails is calculated as described in the following.

The RF of day-time contrails ($RF_{aCCF-day}$ in $[W/m^2]$) is based on the outgoing longwave radiation (OLR) at top of the atmosphere in $[W/m^2]$ at the time and location of the contrail formation. For a specific atmospheric location and time, the $RF_{aCCF-day}$ is given by:

595 $$RF_{aCCF-day}(OLR) = 10^{-10} * (-1.7 - 0.0088 * OLR) \qquad (A4)$$

According to the equation, the RF for the daytime contrails can take positive and negative values, depending on the OLR. The RF of night-time contrails ($RF_{aCCF-night}$) in $[W/m^2]$ is based on temperature (T) in [K]. For an atmospheric location (x,y,z) at time t:

$$RF_{aCCF-night}(T) = 10^{-10} * (0.0073 * 10^{0.0107*T} - 1.03) \qquad (A5)$$

600 For temperatures less than 201 K, the night-time contrail is set to zero. The above calculated RF of contrails can be converted to global temperature change (P-ATR20) by multiplying with a constant factor of 0.0151 $K/(W/m^2)$ (Yin et al., 2022). The resulting contrail aCCFs are then given in temperature change per flown kilometre [K/km].

Contrail aCCFs are only relevant at locations where persistent contrails can form and accordingly regions without persistent contrails have to be set to zero. For that locations in which persistent contrails can form have to be calculated. Persistent

605 contrails can be identified by two conditions: temperature below 235 K and relative humidity with respect to ice at or above 100 % (see supplement of Yin et al., 2022). Alternatively, the more accurate Schmidt-Appleman-criterion (Appleman, 1953), which additionally considers the aircraft engine type, could be used.

CO_2 aCCF

In order to compare these merged non-CO_2 aCCFs to the climate impact of CO_2 a value for a CO_2 aCCFs is calculated with

610 the climate-chemistry response model AirClim (Dahlmann et al., 2016). In case of the pulse scenario used also for the aCCFs

above, the CO_2 is given by $7.48 * 10^{-16} [K/kg(fuel)]$ (Yin et al., 2022). Note, that also the CO_2 aCCFs vary with the used emission scenario.

Appendix B: Additional figures
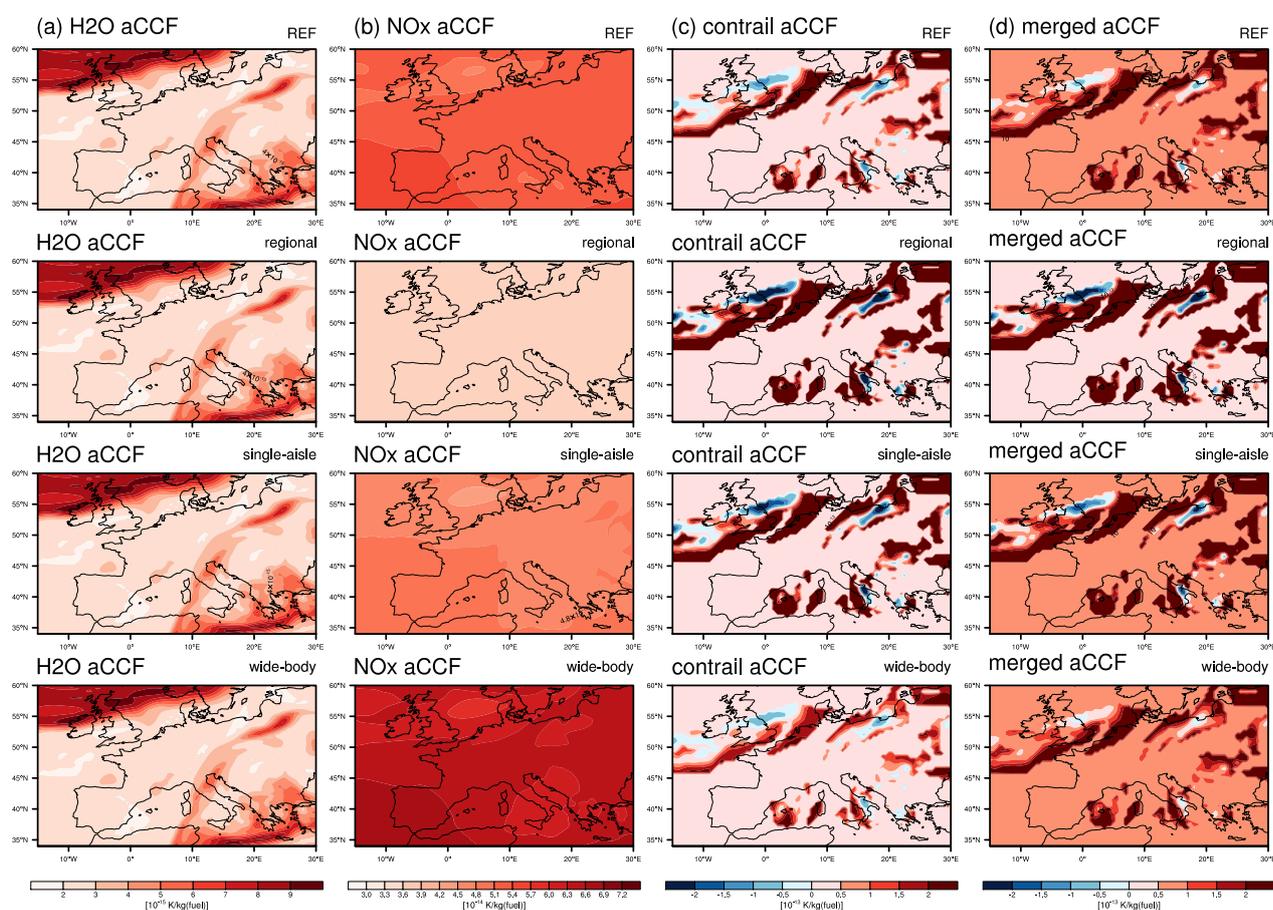
Figure A1. Individual aCCFS of water vapour, NO_x, contrail-cirrus together with merged aCCFs using at pressure level 250 unithPa over Europe on 15th of June 2018 (12 UTC), using four different assumptions for the NO_x emission index and the specific range values (typical transatlantic fleet mean (first row), regional aircraft type (second row), single-aisle aircraft type (third row) and wide-body aircraft type(last row)). Units are all given in [K/kg(fuel)].
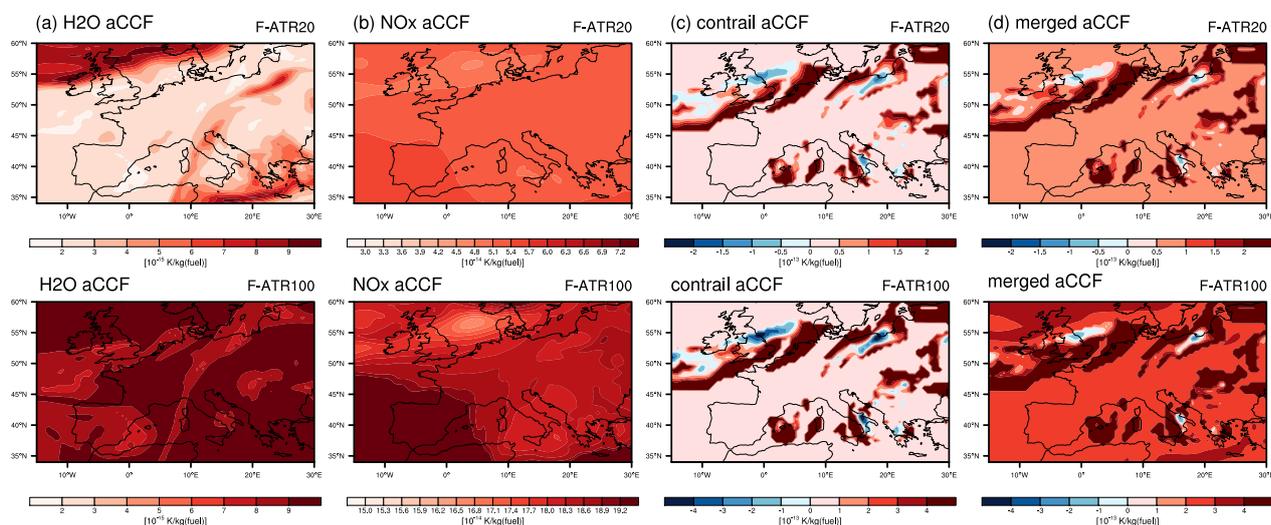
Figure A2. Individual aCCFs of water vapour, NO$_x$, contrail-cirrus together with merged aCCFs using at pressure level 250 unithPa over Europe on 15th of June 2018 (12 UTC), using two different assumptions for the metric: ATR20 and ATR100. Units are all given in [K/kg(fuel)]

References

Appleman, H.: The formation of exhaust condensation trails by jet aircraft, Bulletin of the American Meteorological Society, 34, 14–20,
630   1953.

Bickel, M., Ponater, M., Bock, L., Burkhardt, U., and Reineke, S.: Estimating the effective radiative forcing of contrail cirrus, Journal of
Climate, 33, 1991–2005, 2020.

Castino, F., Yin, F., Grewe, V., Soler, M., Simorgh, A., Yamashita, H., Matthes, S., Baumann, S., Dietmüller, S., Linke, F., et al.: Seasonal
Variability of Aircraft Trajectories reducing NOx-climate Impacts under a Multitude of Weather Patterns, 2021.

635   Cess, R., Potter, G., Blanchet, J., Boer, G., Ghan, S., Kiehl, J., Letreut, H., Li, Z., Liang, X., Mitchell, J., Morcrette, J., Randall, D., Riches, M.,
Roeckner, E., Schlese, U., Slingo, A., Taylor, K., Washington, W., Wetherrald, R., and Yagi, I.: Interpretation of cloud-climate feedback
as produced by 14 atmospheric general-circulation models, Science, 245, 513–516, https://doi.org/10.1126/science.245.4917.513, 1989.

Dahlmann, K., Grewe, V., Frömming, C., and Burkhardt, U.: Can we reliably assess climate mitigation options for air traffic scenarios despite
large uncertainties in atmospheric processes?, Transportation Research Part D: Transport and Environment, 46, 40–55, 2016.

640   Dee, D. P., Uppala, S. M., Simmons, A., Berrisford, P., Poli, P., Kobayashi, S., Andrae, U., Balmaseda, M., Balsamo, G., Bauer, d. P., et al.:
The ERA-Interim reanalysis: Configuration and performance of the data assimilation system, Quarterly Journal of the royal meteorological
society, 137, 553–597, 2011.

DuBois, D. and Paynter, G. C.: " Fuel Flow Method2" for Estimating Aircraft Emissions, SAE Transactions, pp. 1–14, 2006.

Frömming, C., Grewe, V., Brinkop, S., Jöckel, P., Haslerud, A. S., Rosanka, S., van Manen, J., and Matthes, S.: Influence of weather situation
645   on non-CO 2 aviation climate effects: the REACT4C climate change functions, Atmospheric Chemistry and Physics, 21, 9151–9172,
2021.

Fuglestvedt, J. S., Shine, K. P., Berntsen, T., Cook, J., Lee, D., Stenke, A., Skeie, R. B., Velders, G., and Waitz, I.: Transport impacts on
atmosphere and climate: Metrics, Atmospheric Environment, 44, 4648–4677, 2010.

Gierens, K., Matthes, S., and Rohs, S.: How well can persistent contrails be predicted?, Aerospace, 7, 169, 2020.

650   Graver, B. and Rutherford, D.: Transatlantic airline fuel efficiency ranking, 2017, International Council on Clean Transportation, 2018.

Grewe, V. and Dahlmann, K.: How ambiguous are climate metrics? And are we prepared to assess and compare the climate impact of new
air traffic technologies?, Atmospheric Environment, 106, 373–374, 2015.

Grewe, V. and Stenke, A.: AirClim: an efficient tool for climate evaluation of aircraft technology, Atmospheric Chemistry and Physics, 8,
4621–4639, 2008.

655   Grewe, V., Frömming, C., Matthes, S., Brinkop, S., Ponater, M., Dietmüller, S., Jöckel, P., Garny, H., Tsati, E., Dahlmann, K., et al.:
Aircraft routing with minimal climate impact: The REACT4C climate cost function modelling approach (V1. 0), Geoscientific Model
Development, 7, 175–201, 2014.

Grewe, V., Matthes, S., and Dahlmann, K.: The contribution of aviation NOx emissions to climate change: are we ignoring methodological
flaws?, Environmental Research Letters, 14, 121 003, 2019.

660   Hansen, J., Sato, M., Ruedy, R., Nazarenko, L., Lacis, A., Schmidt, G., Russell, G., Aleinov, I., Bauer, M., Bauer, S., et al.: Efficacy of
climate forcings, Journal of geophysical research: atmospheres, 110, 2005.

Irvine, E., Hoskins, B., and Shine, K.: A Lagrangian analysis of ice-supersaturated air over the North Atlantic, Journal of Geophysical
Research: Atmospheres, 119, 90–100, 2014.

Irvine, E. A., Hoskins, B. J., Shine, K. P., Lunnon, R. W., and Froemming, C.: Characterizing North Atlantic weather patterns for climate-
665   optimal aircraft routing, Meteorological Applications, 20, 80–93, 2013.

Jelinek, F.: The Advanced Emission Model (AEM3)-Validation Report, Ratio, 306, 1–13, 2004.

Jöckel, P., Tost, H., Pozzer, A., Kunze, M., Kirner, O., Brenninkmeijer, C. A., Brinkop, S., Cai, D. S., Dyroff, C., Eckstein, J., et al.: Earth
       system chemistry integrated modelling (ESCiMo) with the modular earth submodel system (MESSy) version 2.51, Geoscientific Model
       Development, 9, 1153–1200, 2016.

670   Joshi, M., Shine, K., Ponater, M., and Stuber, N.: A comparison of climate response to different radiative forcings in the general circulation
       models: toward an improved metric of climate change, Clim. Dyn., 20, 843–854, https://doi.org/10.1007/s00382-003-0305-9, 2003.

Lee, D. S., Fahey, D., Skowron, A., Allen, M., Burkhardt, U., Chen, Q., Doherty, S., Freeman, S., Forster, P., Fuglestvedt, J., et al.: The
       contribution of global aviation to anthropogenic climate forcing for 2000 to 2018, Atmospheric Environment, 244, 117 834, 2021.

Linke, F., Grewe, V., and Gollnick, V.: The implications of intermediate stop operations on aviation emissions and climate, Meteorologische
675   Zeitschrift, 26, 697–709, 2017.

Lührs, B., Linke, F., Matthes, S., Grewe, V., and Yin, F.: Climate impact mitigation potential of European air traffic in a weather situation
       with strong contrail formation, Aerospace, 8, 50, 2021.

Marenco, A., Thouret, V., Nédélec, P., Smit, H., Helten, M., Kley, D., Karcher, F., Simon, P., Law, K., Pyle, J., et al.: Measurement of
       ozone and water vapor by Airbus in-service aircraft: The MOZAIC airborne program, An overview, Journal of Geophysical Research:
680   Atmospheres, 103, 25 631–25 642, 1998.

Matthes, S., Grewe, V., Dahlmann, K., Frömming, C., Irvine, E., Lim, L., Linke, F., Lührs, B., Owen, B., Shine, K., et al.: A concept for
       multi-criteria environmental assessment of aircraft trajectories, Aerospace, 4, 42, 2017.

Matthes, S., Lührs, B., Dahlmann, K., Grewe, V., Linke, F., Yin, F., Klingaman, E., and Shine, K. P.: Climate-optimized trajectories and
       robust mitigation potential: Flying ATM4E, Aerospace, 7, 156, 2020.

685   Matthes, S., Dahlmann, K., Dietmüller, S., Yamashita, H., Grewe, V., Soler, M., Simorgh, A., González Arriba, D., Linke, F., Lührs, B.,
       Meuser, Maximilian, C. F., and Yin, F.: Concept for identifying robust eco-efficient aircraft trajectories: methodological concept of climate-
       optimized aircraft trajectories in FlyATM4E, Aerospace, 2022, in preparation.

Nuic, A. and Mouillet, V.: User manual for the base of aircraft data (BADA) family 4, European Organisation for the Safety of Air Navigation
       (EUROCONTROL) TR, 12, 22–58, 2012.

690   Penner, J. E., Lister, D., Griggs, D. J., Dokken, D. J., and McFarland, M.: Aviation and the global atmosphere: a special report of the
       Intergovernmental Panel on Climate Change, 1999.

Petzold, A., Neis, P., Rütimann, M., Rohs, S., Berkes, F., Smit, H. G., Krämer, M., Spelten, N., Spichtinger, P., Nédélec, P., et al.: Ice-
       supersaturated air masses in the northern mid-latitudes from regular in situ observations by passenger aircraft: vertical distribution, sea-
       sonality and tropospheric fingerprint, Atmospheric chemistry and physics, 20, 8157–8179, 2020.

695   Ponater, M., Marquart, S., Sausen, R., and Schumann, U.: On contrail climate sensitivity, Geophysical Research Letters, 32, 2005.

Ponater, M., Pechtl, S., Sausen, R., Schumann, U., and Hüttig, G.: Potential of the cryoplane technology to reduce aircraft climate impact: A
       state-of-the-art assessment, Atmospheric Environment, 40, 6928–6944, 2006.

Pruppacher, H. R., Klett, J. D., and Wang, P. K.: Microphysics of clouds and precipitation, 1998.

Rao, P., Yin, F., Grewe, V., Yamashita, H., Jöckel, P., Matthes, S., Mertens, M., and Frömming, C.: Case Study for Testing the Validity of NO
700   x-Ozone Algorithmic Climate Change Functions for Optimising Flight Trajectories, Aerospace, 9, 231, 2022.

Rap, A., Forster, P. M., Haywood, J. M., Jones, A., and Boucher, O.: Estimating the climate impact of linear contrails using the UK Met Office climate model, Geophysical research letters, 37, 2010.

Simorgh, A., Soler, M., González-Arribas, D., Matthes, S., Grewe, V., Dietmüller, S., Baumann, S., Yamashita, H., Yin, F., Castino, F., Linke, F., Lührs, B., and Meuser, M. M.: A Comprehensive Survey on Recent Climate Optimal Aircraft Trajectory Planning., Aerospace, 9, 143, 2022.

van Manen, J. and Grewe, V.: Algorithmic climate change functions for the use in eco-efficient flight planning, Transportation Research Part D: Transport and Environment, 67, 388–405, 2019.

Yamashita, H., Yin, F., Grewe, V., Jöckel, P., Matthes, S., Kern, B., Dahlmann, K., and Frömming, C.: Newly developed aircraft routing options for air traffic simulation in the chemistry–climate model EMAC 2.53: AirTraf 2.0, Geoscientific Model Development, 13, 4869–4890, 2020.

Yamashita, H., Yin, F., Grewe, V., Jöckel, P., Matthes, S., Kern, B., Dahlmann, K., and Frömming, C.: Analysis of aircraft routing strategies for north atlantic flights by using airtraf 2.0, Aerospace, 8, 33, 2021.

Yin, F., Grewe, V., Castino, F., Rao, P., Matthes, S., Yamashita, H., Dahlmann, K., Frömming, C., Dietmüller, S., Peter, Patrick Klingaman, E., Shine, K., Lührs, B., and Linke, F.: Predicting the climate impact of aviation for en-route emissions: The algorithmic climate change function sub model ACCF 1.0 of EMAC 2.53, submission to GMDD in August 2022, 2022.